MULTIDISCIPLINARY OPTIMIZATION OF SPACE PLANE MODELED AS RIGID BODY

Nobuhiro Yokoyama*
***Department of Aeronautics and Astronautics, University of Tokyo**

Keywords: *Multidisciplinary Design Optimization, Direct Collocation, Metamodeling, Trim, Stability*

Abstract

Conceptual design of a space plane is a multidisciplinary process that is characterized by many variables. A Multidisciplinary Design Optimization (MDO) problem of a single-stage-to-orbit (SSTO) space plane is formulated and solved in this study. Special attentions are paid to the modeling and the optimization of the rigid body characteristics such as the trim capability and the stability, because the space plane has a tendency of considerable migration of the aerodynamic center and the center of gravity. Computational intractability of the MDO problem is circumvented by Direct Collocation with singular perturbation as well as the metamodeling of aerodynamics. Trajectory and design of the vehicle optimized by the MDO technique are presented, and their relationships with the rigid body characteristics are investigated.

1 Introduction

A fully reusable, winged space plane is one of the promising candidates for the future space transportation system, in which the cost reduction and the reliability enhancement are the principal goals. The key feature of the space plane is that the entire system is composed of various disciplines that interact with one another. Thus, Multidisciplinary Design Optimization (MDO), which integrates the simulation tools of constituent disciplines and optimizes the entire system, offers a great advantage to the conceptual design. There are several advanced MDO methods such as Concurrent Subspace Optimization [1] or Collaborative Optimization [2], and a number of MDO applications to the conceptual design of space planes are reported [2-5].

To obtain practical results by MDO, the analysis tool of each discipline should support sufficiently accurate and reliable model. In view of flight dynamics, it is important to support the rigid body characteristics such as the trim capability and the stability. In particular, winged space planes have a tendency of considerable migration in both the aerodynamic center and the center of gravity (c.g.) as it accelerates from take-off velocity to orbital velocity. The migration can cause severe instability and produce large moments that must be counteracted [6]. Nevertheless, in the past MDO studies of winged space planes, the optimization of these rigid body characteristics has rarely been considered in detail. Therefore, this study formulates and solves the MDO problem of a winged single-stage-to-orbit (SSTO) space plane covering the rigid body characteristics.

In this study, special attentions are paid to the modeling of the dynamics related to the trim and the stability, i.e., the following new approaches are introduced to circumvent the computational intractability and obtain the optimal solution successfully. 1) To alleviate the stiffness of the state equations inherent in the rigid body dynamics, Direct Collocation [7] incorporating the singular perturbation [8] is adopted. In this approach, the differential equation of a small time scale variable is converted to an algebraic equality constraint, and the stability condition is imposed as an algebraic inequality constraint. Then the

trajectory optimization problem of the resulting differential algebraic equations (DAEs) is solved by applying an implicit numerical integration. 2) It is computationally costly to calculate the aerodynamics with high-precision analysis methods in every optimization step. In particular, to design the vehicle that has desirable aerodynamic characteristics in view of the trim and the stability, many design variables should be handled simultaneously. Therefore, metamodels [9], that mathematically approximate the input-output relationship sampled by the original analyses, are used as the substitutes for the original analyses.

Using the MDO incorporating the above approaches, the conceptual design of the vehicle and its flight trajectory are optimized. Moreover, the relationships between the rigid body characteristics and the optimal solution are investigated.

2 Statement of the Problem

2.1 Overview of the MDO Problem

A conceptual design optimization problem of a horizontal take-off, horizontal landing SSTO is considered. Taking the runway off, the vehicle targets a circular orbit at an altitude of 100 km. The take-off mass of the vehicle is assumed to be 500 Mg. One of the most important performance criteria of SSTO is its capability of payload transportation. Therefore, the objective function to be maximized in the MDO is the payload mass ratio ϕ defined as follows:

$$\phi = \frac{m_0 - m_E}{m_0} \rightarrow \text{maximize} \qquad (1)$$

where m_0 is the specified take-off mass (= 500 Mg) and m_E is the estimated total mass excluding the payload mass. That is, the value of $m_0 - m_E$ corresponds to the payload mass. It should be noted that if optimal ϕ is a negative value, the vehicle is still technically infeasible under the simulation models assumed in this study and it means assumption of further technological advance is necessary to achieve the feasible design.

As shown in fig. 1, the MDO architecture is implemented by the interaction between an analysis process and an optimization process. Furthermore, the analysis process consists of four disciplines as outlined in the following subsections. In this study, the analyses of constituent disciplines were carried out in all-at-once manner, unlike the decomposition-based analyses [1, 2]. This all-at-once approach was enabled by the automation of all the analyses.

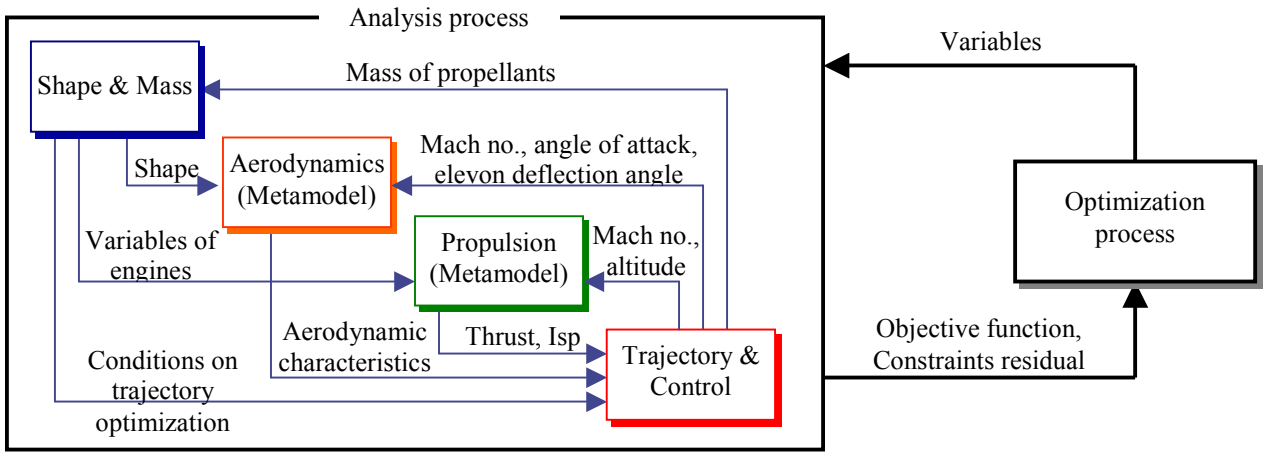

Fig. 1. Schematic view of MDO

2.2 Shape and Mass

Figure 2 shows the basic configuration of the SSTO space plane as well as the shape design variables to be optimized. The basic configuration is based on ref. [10] to attain favorable propulsion performance. The wing section is NACA0006. The elevons are assumed to be 40 % of the wing tip chord, and 80 % of the exposed wing semi-span. The total area of two vertical tails is assumed as 13 % of the wing area. As propulsion system, six pre-cooled turbojet engines (PCTJ) [11] are mounted on the bottom side of the body, and four rocket engines (ROC) are mounted on the base side of the body. As propellants, liquid hydrogen (LH_2) is loaded in tanks made of composite materials, and liquid oxygen (LOX) is loaded in a tank made of aluminum alloy. Some LH_2 tanks are located in front of the LOX tank, and the others are located in rear of the LOX tank. The average cross-sectional areas of the tanks are assumed to be less than 60% of the cross-sectional area of the fuselage. Lengths and locations of the tanks are also designed in the framework of MDO. As the other variables of the vehicle, the maximum dynamic pressure, the maximum load factor, the maximum axial acceleration (= acceleration with respect to the body axis), the total capture area and the maximum thrust of PCTJ, and the vacuum thrust ROC are designed.

Mass of the components is estimated by the statistical equations [12, 13]. The c.g. of the vehicle is calculated on the basis of mass estimation results and locations of components.

2.3 Trajectory and Control

An ascent trajectory optimization problem considering the rigid body characteristics is solved. For simplicity, the motion of the vehicle is supposed to be constrained on the equatorial plane, and only the longitudinal dynamics is considered. The flight sequence is specified as follows. 1) The vehicle takes the runway off propelled by PCTJ. The total take-off distance is restrained within 3500m. 2) The vehicle is accelerated by PCTJ until its flight Mach number reaches 6.0, i.e., the operational limit of the PCTJ. 3) When the flight Mach number

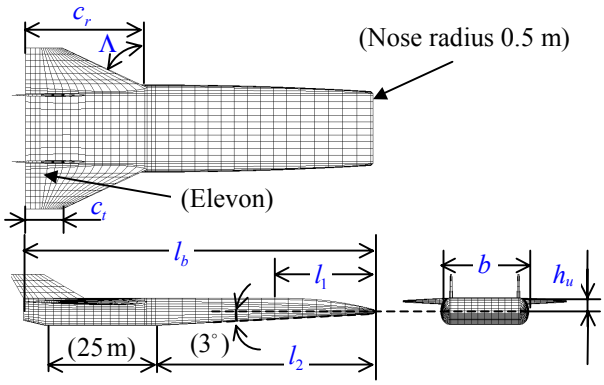

Fig. 2. Basic configuration of the vehicle and the shape design variables to be optimized

reaches 6.0, the operating engine is switched from PCTJ to ROC and the vehicle is accelerated further. 4) At an altitude above 90 km, ROC is cut off and the vehicle begins coasting. 5) At the orbital altitude of 100km, ROC is re-ignited to accelerate the vehicle to the orbital velocity.

The motion of the vehicle is controlled by 1) the elevon deflection angle δ_e during the flight with PCTJ, 2) the thrust T_R and the thrust vector angle δ_R of ROC during the flight with ROC. Furthermore, it is assumed possible to control the proportions of LH_2 consumptions at the forward and rear tanks, and hence the optimal control of the c.g. position is also supported. The motion of the vehicle considering the rigid body dynamics is defined by the following set of differential equations.

$$\dot{m}_{HF} = -\left(\frac{T_P}{I_P} + \frac{1}{1+\lambda}\frac{T_R}{I_R}\right)\frac{\varepsilon}{g_0} \tag{2}$$

$$\dot{m}_{HR} = -\left(\frac{T_P}{I_P} + \frac{1}{1+\lambda}\frac{T_R}{I_R}\right)\frac{1-\varepsilon}{g_0} \tag{3}$$

$$\dot{m}_O = -\left(\frac{T_P}{I_P} + \frac{\lambda}{1+\lambda}\frac{T_R}{I_R}\right)\frac{1}{g_0} \tag{4}$$

$$\dot{r}\left(=\dot{h}\right) = v\sin\gamma \tag{5}$$

$$\dot{v} = \left[T_P\cos\alpha + T_R\cos(\alpha+\delta_R) - D\right]/m - g\sin\gamma \tag{6}$$

$$\dot{\gamma} = \left[L + T_P \sin\alpha + T_R \sin(\alpha + \delta_R)\right]/mv + (v/r - g/v)\cos\gamma + 2\omega \tag{7}$$

$$\dot{\alpha} = -\dot{\gamma} + q \tag{8}$$

$$\dot{q} = [\underline{M} - (L\cos\alpha + D\sin\alpha)(x_{ref} - x_{cg}) - T_R(x_R - x_{cg})\sin\delta_R]/I_{yy} = 0 \tag{9}$$

where the variables are defined as follows. m_{HF} : mass of remaining LH_2 in the forward tanks, m_{HR} : mass of remaining LH_2 in the rear tanks, m_O : mass of remaining LOX, r : geocentric distance, h : altitude, v : velocity, γ : flight-path angle, α : angle of attack, q : pitch rate, m : mass of the vehicle, x_{cg} : c.g. position of the vehicle, x_{ref} : aerodynamic reference point, I_{yy} : moment of inertia with respect to the pitch axis, L : lift, D : drag, $\underline{M}$: aerodynamic pitching moment acting on x_{ref} , T_P : thrust of PCTJ, I_P : specific impulse of PCTJ, I_R : specific impulse of ROC, x_R : thrust action point of ROC, ε : proportion of LH_2 consumption at the forward tanks, λ : LOX/LH_2 mixture ratio of ROC (=6.0), g : acceleration of gravity ($=\mu/r^2 - r\omega^2$), μ : gravitational constant of the earth ($=3.986\times10^{14}\,[\mathrm{m^3/s^2}]$), ω : angular velocity of the rotation of the earth ($=7.277\times10^{-5}\,[\mathrm{rad/s}]$), g_0 : acceleration of gravity at sea level (= 9.80655 $[\mathrm{m/s^2}]$) . The x-axis corresponds to the body axis and its origin is located on the nose of the vehicle. For simplicity, the pitching moment produced by PCTJ is neglected and only the c.g. position with respect to x-axis is considered.

The state equations (2)-(9) tend to be a stiff system, because the time scale of the pitch rate q is considerably smaller than those of the other state variables. The stiffness of the system often makes it difficult to solve the trajectory optimization problem. Therefore, the singular perturbation approach [8] is adopted in this study, i.e., it is assumed that the pitch rate q is settled at any time of the flight, i.e., $dq/dt = 0$, and it is also assumed that any angle of attack α can be attained in no time by the control system. Then the state equations are converted to DAEs composed of (2)-(7) and the following equation.

$$\underline{M} - (L\cos\alpha + D\sin\alpha)(x_{ref} - x_{cg}) - T_R(x_R - x_{cg})\sin\delta_R = 0 \tag{10}$$

Equation (10) actually means the static trim condition. The converted DAEs are relatively easy to solve due to relieved stiffness, and the contributions of the original dynamics (9) to the flight performances are approximately covered by the equation (10).

The control variables and their lower/upper limits are defined as follows.

$$0 \le \alpha \le 20\,[\mathrm{deg}], 0 \le T_R \le T_{R\max}, 0 \le \varepsilon \le 1$$
$$-10 \le \delta_e \le 10\,[\mathrm{deg}], -10 \le \delta_R \le 10\,[\mathrm{deg}], \tag{11}$$

It should be noted that the angle of attack α is actually bound by the other control variables in the equality condition (10).

Throughout the flight, the following variables are constrained to be less than their designed maximum values: thrust of PCTJ and ROC, the dynamic pressure, the load factor, and the axial acceleration. In addition, the aerodynamic stability condition defined by the following inequality is also imposed.

$$x_{ac} \ge x_{cg} \tag{12}$$

where x_{ac} denotes the aerodynamic center and is calculated based on the aerodynamic coefficients.

2.4 Aerodynamics Characteristics

The lift coefficient C_L, the drag coefficient C_D, and the pitching moment coefficient C_m are calculated based on the combinations of representative values of the Mach number M, the angle of attack α, and the elevon deflection angle δ_e as shown in table 1. If a shape of the vehicle is given, the aerodynamic coefficients are obtained by the linear interpolation of the representative M and polynomial interpolation of α as well as δ_e in the following form:

$$C_L = C_{L0} + C_{L1}\alpha + C_{L2}\alpha^2 + C_{L3}\delta_e + C_{L4}\delta_e^2 + C_{L5}\alpha\delta_e + C_{L6}\alpha^2\delta_e + C_{L7}\alpha\delta_e^2 + C_{L8}\alpha^2\delta_e^2 \tag{13}$$

where the parameters $C_{L0},\cdots,C_{L8}$ are the function of the shape design variables. The other coefficients C_D and C_m are also modeled in the same way as (13). These models for the aerodynamic coefficients support the contribution of the incidental force produced by the elevon deflection.

The linear potential flows are calculated by the panel method [14] at subsonic and supersonic regime. The Prandtl-Meyer expansion flow theory and the tangent cone/wedge methods [15] are applied at hypersonic regime. In both cases, the skin friction drag is estimated by Sommer and Short T′ semi-empirical method [16]. The base drag is estimated by empirical equations [15]. Moreover, the aerodynamic characteristics at the representative Mach number of transonic regime ($M=1.05$) are assumed to be the same as those at $M=1.2$. Compared to recent Computational Fluid Dynamics (CFD), the methods used in this study are less accurate, but they have advantages in the following aspects. 1) It is relatively easy to implement a tool for automatic generation of shape grid needed for the aerodynamic calculations. 2) While the computational costs for CFD approaches are usually high, those for the methods used in this study are moderate. Nevertheless, these methods still consume much computational time if they are directly applied in the framework of MDO, because numerous numbers of cases must be calculated. Therefore, metamodels are introduced to reduce the computational time for the aerodynamic calculations. The metamodel construction methodology is given in section 3.2.

2.5 Propulsion Performances

The thrust and the specific impulse of the engines are calculated on the basis of the design parameters for propulsion system, i.e., total capture area of PCTJ, and vacuum thrust of ROC.

Performance analysis of PCTJ is based on ref. [11]. The thrust per unit capture area and the specific impulse of PCTJ are given in the form of map data with respect to the Mach number and the altitude. The map data are approximated by the metamodels to apply in the framework of MDO. The thrust and the specific impulse of ROC are modeled as the functions of the altitude. Vacuum specific impulse of ROC is assumed as 450 sec.

Table 1. Representative values of the flight condition parameters for aerodynamic analysis

Parameters	Representative values
M	0.2, 0.7, 0.9, 1.05, 1.2, 6, 10, 15, 20, 30
α	0, 10, 20 [deg]
δ_e	-10, 0, 10 [deg]

3 Methods for Optimization

3.1 Direct Collocation with Sparse SQP

Since the trajectory optimization problem is composed of the dynamic system as described in the section 2.3, Direct Collocation [7] is applied to convert the trajectory optimization problem into a nonlinear programming (NLP) problem. Then the trajectory optimization problem and the design optimization problem are formulated in a set of NLP problem. The outlines are as follows.

Discretizing the time domain $[t_0,t_f]$ into $N+1$ grid points as $t_0,t_1,\cdots,t_N(=t_f)$, let us denote the state variable $\boldsymbol{x}(t_i)$ and the control variable $\boldsymbol{u}(t_i)$ as $\boldsymbol{x}_i,\boldsymbol{u}_i\ (i=0,1,\cdots,N)$. Moreover, let us define the static variables (such as the terminal time and the design variables of the vehicle) as $\boldsymbol{p}$. Then the NLP problem is formulated as follows.

- Variables to be optimized:

$$\boldsymbol{x}_0,\boldsymbol{u}_0,\bar{\boldsymbol{x}}_1,\bar{\boldsymbol{u}}_1,\boldsymbol{x}_1,\boldsymbol{u}_1,\cdots,\bar{\boldsymbol{x}}_N,\bar{\boldsymbol{u}}_N,\boldsymbol{x}_N,\boldsymbol{u}_N,\boldsymbol{p} \quad (14)$$

where $\bar{\boldsymbol{x}}_i\equiv\boldsymbol{x}((t_{i+1}+t_i)/2)$, $\bar{\boldsymbol{u}}_i\equiv\boldsymbol{u}((t_{i+1}+t_i)/2)$.

- Objective function:

$$\phi(\boldsymbol{x}_N,\boldsymbol{u}_N,\boldsymbol{p})\rightarrow\text{maximize} \quad (15)$$

- Initial conditions at time $t=t_0$:

$$\boldsymbol{\psi}_0(\boldsymbol{x}_0,\boldsymbol{u}_0,\boldsymbol{p})=\boldsymbol{0},\boldsymbol{\chi}_0(\boldsymbol{x}_0,\boldsymbol{u}_0,\boldsymbol{p})\geq\boldsymbol{0} \quad (16)$$

- Equality constraints for implicit numerical

integration of the state equations (Separated Hermite-Simpson rule [7]):

$$\left.\begin{aligned} \bar{\boldsymbol{x}}_i - \frac{\boldsymbol{x}_{i+1}+\boldsymbol{x}_i}{2} - \frac{\boldsymbol{f}_i - \boldsymbol{f}_{i+1}}{8}\Delta t_i = \boldsymbol{0} \\ \boldsymbol{x}_{i+1} - \boldsymbol{x}_i - \frac{\boldsymbol{f}_i + 4\bar{\boldsymbol{f}}_{i+1} + \boldsymbol{f}_{i+1}}{6}\Delta t_i = \boldsymbol{0} \end{aligned}\right\} \quad (i = 0,\cdots,N-1) \tag{17}$$

where $\boldsymbol{f}_i \equiv \boldsymbol{f}(\boldsymbol{x}_i, \boldsymbol{u}_i, \boldsymbol{p})$, $\bar{\boldsymbol{f}}_i \equiv \boldsymbol{f}(\bar{\boldsymbol{x}}_i, \bar{\boldsymbol{u}}_i, \boldsymbol{p})$ denotes the state equations, and Δt_i denotes the time duration $t_{i+1} - t_i$.

- Path constraints:

$$\begin{aligned} &\boldsymbol{c}(\boldsymbol{x}_i, \boldsymbol{u}_i, \boldsymbol{p}) = \boldsymbol{0},\ \boldsymbol{s}(\boldsymbol{x}_i, \boldsymbol{u}_i, \boldsymbol{p}) \geq \boldsymbol{0} \quad (i = 0,\cdots,N) \\ &\boldsymbol{c}(\bar{\boldsymbol{x}}_i, \bar{\boldsymbol{u}}_i, \boldsymbol{p}) = \boldsymbol{0},\ \boldsymbol{s}(\bar{\boldsymbol{x}}_i, \bar{\boldsymbol{u}}_i, \boldsymbol{p}) \geq \boldsymbol{0} \quad (i = 1,\cdots,N) \end{aligned} \tag{18}$$

- Terminal conditions at time $t = t_{\mathrm{f}}$:

$$\boldsymbol{\psi}_{\mathrm{f}}(\boldsymbol{x}_N, \boldsymbol{u}_N, \boldsymbol{p}) = \boldsymbol{0},\ \boldsymbol{\chi}_{\mathrm{f}}(\boldsymbol{x}_N, \boldsymbol{u}_N, \boldsymbol{p}) \geq \boldsymbol{0} \tag{19}$$

- Constraints for static variables:

$$\boldsymbol{g}(\boldsymbol{p}) = \boldsymbol{0},\ \boldsymbol{h}(\boldsymbol{p}) \geq \boldsymbol{0} \tag{20}$$

Equation (20) involves all the constraints on the analyses of shape, mass, aerodynamics, and propulsion.

Unlike the trajectory optimization based on an explicit integration approach such as Direct Shooting, Direct Collocation robustly solves DAEs formulated in the form of (2)-(7) and (10). On the other hand, it has a disadvantage that the resulting NLP problem has a large number of variables and constraints. Nevertheless, a Sparse Sequential Quadratic Programming (Sparse SQP) is applied to exploit the sparsity of the resulting Hessian and Jacobian in the NLP problem, and hence it substantially reduces the computational time compared to conventional optimization approaches.

3.2 Metamodeling

3.2.1 Radial Basis Function

To reduce the computational cost for the analyses of the aerodynamic characteristics and the propulsion performances, the metamodels are used as the substitutes for the original analyses. Although there are some candidates for the metamodel such as polynomial regression, neural network, or Kriging [9], Radial Basis Function (RBF) [18] was employed as the metamodel in this study. The RBF has the following advantages. 1) Fitting algorithms and validation methodologies for robust approximation are substantially simpler than those used for neural networks or Kriging, because the RBF is a linear combination of bases like polynomial regression. 2) While the selection of bases in polynomial regression is cumbersome as the input dimension or the output nonlinearity increases, the selection of bases in RBF can be automated easily.

Let us denote the inputs and the output as $\boldsymbol{x}$ and $f(\boldsymbol{x})$ respectively. Then the RBF metamodel used in this study is expressed as the linear combination of the Gaussian:

$$f(\boldsymbol{x}) = \sum_{i=1}^{N} w_i \exp\left(-\| \boldsymbol{x} - \boldsymbol{c}_i \|^2 / \beta^2\right) \tag{21}$$

where $w_1,\cdots,w_N$ are weight parameters of the Gaussian, $\boldsymbol{c}_1,\cdots,\boldsymbol{c}_N$ are N sample inputs, and β is the radius of the Gaussian. Orthogonal Least Squares algorithm [17] was applied to determine the weight parameters. Furthermore, to attain robust approximation performance, an optimal radius β is determined based on the Leave-One-Out Cross Validation (LOOCV) [18]. In LOOCV, the N sample data are divided into $(N-1)$ data for temporal fitting and one datum for test. Then the mean squared error (MSE) on the test data over the N possible ways is used as the performance index to evaluate the approximation robustness. The advantage of the LOOCV is that all the sample data is used for fitting as well as evaluating the approximation robustness.

3.2.2 Experimental Design and Metamodel Construction

Experimental designs, that determine the arrangement of sample inputs in the design space, also play an important role to attain robust approximation performance of the metamodels, if the dimension of the inputs or the nonlinearity of the output is high. This was the case with the metamodels for the aerodynamic characteristics due to its high

dimension of the inputs. On the other hand, the elaborate experimental designs were not necessary for the metamodels of the propulsion performances, because sufficient numbers of sample data with respect to two-dimensional inputs were available.

The design space for the aerodynamics analysis was defined by the constraints as shown in table 2. To arrange the sample inputs effectively in the constrained design space, an experimental design referred to as Constrained Sub-Uniform Design (CSUD) [18] was used. CSUD arranges the inputs approximately uniformly in the constrained design space and on each input axis. Preparing 200 sample shapes of the vehicle by CSUD, the aerodynamic characteristics were calculated on each shape and each representative value of the flight condition parameters. Based on these sample data, the metamodels for the aerodynamic coefficients were constructed. In addition, the aerodynamic characteristics of another 200 shapes of the vehicle were calculated. These extra data were sampled at random in the constrained design space, and they were used just to check the approximation robustness of the constructed metamodels. Results indicated that all the metamodels cleared the criterion of the acceptable approximation performance specified as

$$\frac{\sum_{i=1}^{200}[f(\tilde{\boldsymbol{x}}_i)-\tilde{y}_i]^2}{\sum_{i=1}^{200}\tilde{y}_i^2-\left(\sum_{i=1}^{N}\tilde{y}_i\right)^2\Big/200}\le 0.01 \qquad (22)$$

where $\tilde{\boldsymbol{x}}_i, \tilde{y}_i$ $(i=1,\cdots,200)$ denote the inputs and outputs of the test data, and $f(\tilde{\boldsymbol{x}}_i)$ denotes the output obtained by the constructed metamodel. The left hand side of (22) corresponds to the approximation error of the constructed metamodel normalized by the variance inherent in the outputs of the original analysis.

4 Results and Discussion

As the nominal case of the MDO, the aerodynamic stability of the vehicle described as (12) was supposed to be sustained until the flight Mach number reached 8.0. This Mach number was based on the safe side of the maximum Mach number of the PCTJ phase ($M=6.0$) until which the flight with high dynamic pressure is surely required.

Table 2. Major constraints on the shape design

Number	Description
1	$9 \le b \le 19$[m]
2	$2 \le h_u \le 6$[m]
3	$60 \le l_b \le 100$[m]
4	$0.2l_b \le l_1 \le 0.8l_b$[m]
5	$0.6l_b - 12.5 \le l_2 \le l_b - 30.0$[m]
6	$60 \le \Lambda \le 75$[deg]
7	$20 \le c_r \le 50$[m]
8	$0.1c_r \le c_t \le 0.4c_r$[m]
9	$l_1 + c_r + 0.5 \le l_b$[m]
10	$2000 \le$ *Fuselage volume* ≤ 4000[m^3]
11	$300 \le$ *Wing area* ≤ 1500[m^2]

The h-M profile up to $M=10.0$ is shown in fig. 3. During the PCTJ phase, the acceleration was performed along the maximum dynamic pressure line or the maximum thrust line. This h-M profile resulted from the assumption that the thrust control of PCTJ was achieved only by the flight dynamic pressure. If the control of the equivalence ratio of PCTJ is also assumed, the h-M profile may rigidly attach the maximum dynamic pressure line to achieve desirable propulsion performance. The vehicle maneuvered immediately after the operating engine was switched to ROC, which occurred at $M=6.0$. Figure 4 shows the time histories of the control variables α, δ_e, δ_R, and T_R. The trim was attained throughout the flight, and it can be seen in fig. 4 that the control variables were restrained within their acceptable ranges as specified in (11). The thrust of ROC T_R was controlled not to exceed the maximum axial acceleration.

Figure 5 shows the migration profile of the aerodynamic center and the control profile of the c.g. with respect to the flight Mach number. The aerodynamic center moved rearward up to the transonic regime and it moved forward

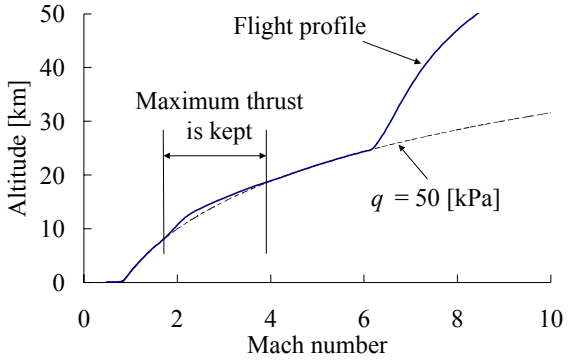

Fig. 3. *h-M* profile (nominal case)

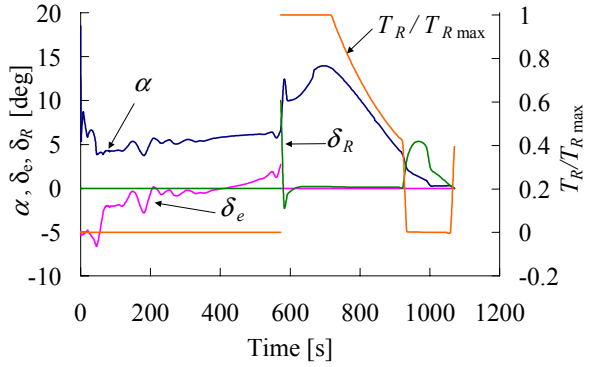

Fig. 4. Time histories of control variables (nominal case)

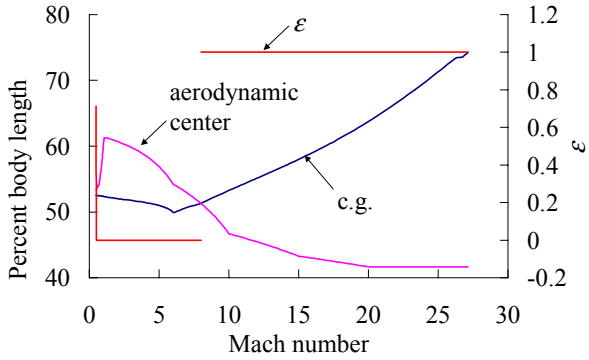

Fig. 5. Migration profile of aerodynamic center and control profile of c.g. (nominal case)

thereafter. This is a typical aerodynamic feature of the space planes [6]. Except for the take-off phase, only the LH_2 in the rear tanks was burned-off (i.e., $\varepsilon = 0$ was kept) up to $M = 8.0$, which was the limit Mach number of the stability. In addition, the amount of LH_2 in the rear tanks was just exhausted at $M = 8.0$. By this control strategy of ε, the c.g. of the vehicle was kept as forward as possible to sustain the aerodynamic stability.

Table 3. Specifications of the vehicle (nominal case)

Payload mass ratio	-0.1340
Total capture area of PCTJ [m^2]	25.40
Maximum thrust of PCTJ [MN]	3.485
Total vacuum thrust of ROC [MN]	5.009
Maximum dynamic pressure [kPa]	50.00
Maximum load factor	2.500
Maximum axial acceleration	1.919
Volume of forward LH_2 tanks [m^3]	4.720×10^2
Volume of rear LH_2 tanks [m^3]	1.182×10^3
Volume of LOX tank [m^3]	2.418×10^2
Body length l_b [m]	61.77
Forebody length (upper side) l_1 [m]	30.36
Forebody length (lower side) l_2 [m]	31.77
Body width b [m]	17.41
Body height of upper side h_u [m]	2.114
Wing sweepback angle Λ [deg]	60.00
Wing root chord length c_r [m]	20.00
Wing tip chord length c_t [m]	7.232

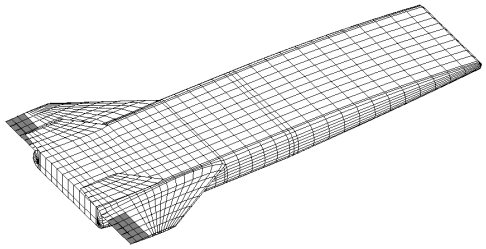

Fig. 6. Shape of the vehicle (nominal case)

The specifications and the shape of the designed vehicle are shown in table 3 and fig. 6 respectively. The payload mass ratio became negative. As mentioned, this result indicates the assumption of further technological advance is necessary to achieve the feasible design. The vehicle has large body width to mount PCTJ on the bottom side of the body, and has small wing to reduce the total mass of the vehicle. Table 4 shows the breakdown of the mass. As can be seen, the mass of PCTJ accounts for a large portion of the dry mass. Thus, comparison of the payload mass ratio with another propulsion options, such as scramjet engine, will be necessary to find the optimal choice of the propulsion system for the SSTO space plane.

Table 4. Breakdown of the mass (nominal case)

Components	Mass [Mg]
Fuselage	24.61
Wing	11.02
Tail	2.98
Landing gear	25.71
Thermal protection system	7.35
PCTJ with thrust structure	51.08
ROC with thrust structure	9.77
Tanks	16.42
Other components	11.68
Dry mass (sum of the above)	160.61
LH_2	117.45
LOX	277.86
Propellants for reentry	11.08
Total mass of the vehicle	567.00

To clarify the relationship between the design of the vehicle and its stability, the limit Mach number of stability was changed to 7.0, 7.5, 8.5, 9.0, and the MDO solution in each case was obtained. Figure 7 and figure 8 show the comparison of the aerodynamic center and the c.g. respectively. It can be seen that as the limit Mach number of stability became demanding, the migration of the aerodynamic center was substantially restrained and the c.g. shifted forward to attain the aerodynamic stability up to the limit Mach number.

Table 5 shows the change of the shape design variables with respect to the limit Mach number of stability. As the stability condition became more demanding, the body section became more planular shape, i.e., b/h_u became large. With respect to the wing shape, the changes of the wing sweepback angle Λ and the wing root chord length c_r were little, while the wing tip chord length c_t became large to make the elevon area large. Figure 9 shows the sensitivity of the payload mass ratio with respect to the limit Mach number of stability. The more the stability condition became demanding, the worse the payload mass ratio became. On the other hand, it was impossible to obtain a solution in which the limit Mach number of stability was more than 9.5. To

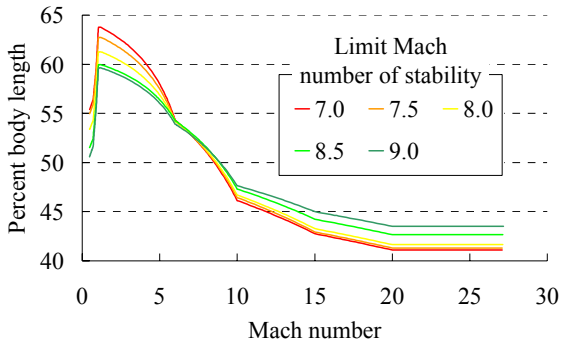

Fig. 7. Comparison of the aerodynamic center

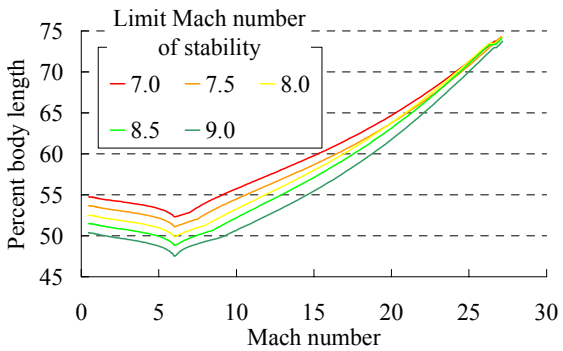

Fig. 8. Comparison of the c.g.

Table 5. Comparison of the shape design variables

Limit Mach number of stability	7.0	8.0	9.0
l_b [m]	60.40	61.77	62.24
l_1 [m]	30.86	30.36	36.67
l_2 [m]	30.32	31.77	32.15
b [m]	16.40	17.41	18.47
h_u [m]	2.569	2.114	2.000
Λ [deg]	60.00	60.00	60.00
c_r [m]	20.44	20.00	20.00
c_t [m]	6.774	7.232	8.000

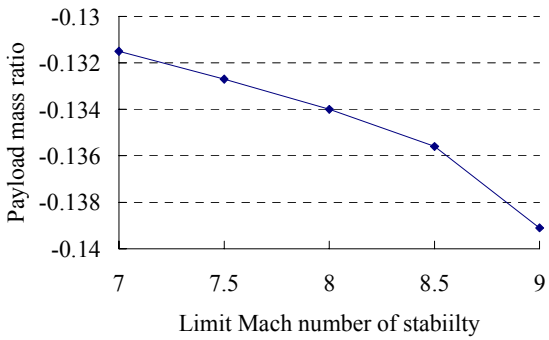

Fig. 9. Sensitivity of the payload mass ratio

design the vehicle that sustains the aerodynamic stability up to higher Mach number, it will be necessary to cover more flexible shape design of the vehicle, such as treating double delta wing and shrinking forebody.

5 Conclusions

This study formulated and solved a Multidisciplinary Design Optimization (MDO) problem of a single-stage-to-orbit (SSTO) space plane considering the trim and the stability. Results indicated that the MDO technique successfully worked to design the vehicle that has the trim capability throughout the flight and the stability during the flight with high dynamic pressure, while it was impossible to design the vehicle that has the stability throughout the flight. In addition, it was observed that there were a trade-off between the payload mass ratio and the stability requirement.

To design more realistic SSTO space plane, a comparative study of the propulsion systems as well as more accurate and flexible modeling of the design problem will be carried out in the near future.

Acknowledgement

This study was supported by a grant from the Japan Society for the Promotion of Science.

The author wishes to thank Hideyuki Taguchi of Japan Aerospace Exploration Agency for providing the data of PCTJ.

References

[1] Sobieski J. Optimization by decomposition - a step from hierarchic to nonhierarchic systems. NASA CP-3031, Part 1, 1989.

[2] Braun R, Moore A and Kroo I. Collaborative approach to launch vehicle design. *Journal of Spacecraft and Rockets*, Vol. 34, No. 4, pp 478-486, 1997.

[3] Rowell L, Braun R, Olds J and Unal R. Multidisciplinary conceptual design optimization of space transportation systems. *Journal of Aircraft*, Vol. 36, No. 1, pp 218-226, 1999.

[4] Tartabini P, Wurster K, Korte J and Lepsch R. Multidisciplinary analysis of a lifting body launch vehicle. *Journal of Spacecraft and Rockets*, Vol. 39, No. 5, pp 788-795, 2002.

[5] Tava M and Suzuki S. Multidisciplinary design optimization of the shape and trajectory of a reentry vehicle. *Transactions of the Japan Society for Aeronautical and Space Sciences*, Vol. 47, No. 155, pp 10-19, 2002.

[6] Shaughnessy J and Gregory I. Trim drag reduction concepts for horizontal takeoff single-stage-to-orbit vehicles. NASA-TM 102687, 1991.

[7] Betts J. *Practical Methods for Optimal Control Using Nonlinear Programming*. 1st edition, SIAM, 2001.

[8] Naidu D and Calise A. Singular perturbations and time scales in guidance and control of aerospace systems: a survey. *Journal of Guidance, Control, and Dynamics*, Vol. 24, No. 6, pp 1057-1078, 2001.

[9] Meckesheimer M, Booker A, Barton R and Simpson T. Computationally inexpensive metamodel assessment strategies. *AIAA Journal*, Vol. 40, No. 10, pp 2053-2060, 2002.

[10] Kanda T and Kudo K. Conceptual study of a combined-cycle engine for an aerospace plane. *Journal of Propulsion and Power*, Vol. 19, No. 5, pp 859-867, 2003.

[11] Taguchi H, Maita M, Yatsuyanagi N and Yanamaka T. Airbreather/rocket combined propulsion systems research for Japanese SSTO spaceplane. AIAA Paper 99-4811, 1999.

[12] Harloff G and Berkowitz B. HASA - hypersonic aerospace sizing analysis for the preliminary design of aerospace vehicles. NASA CR-182226, 1988.

[13] Glatt C. WAATS - a computer program for weights analysis of advanced transportation systems. NASA CR-2420, 1974.

[14] Epton M and Magnus A. PAN AIR – a computer program for predicting subsonic or supersonic linear potential flows about arbitrary configurations using a higher order panel method. NASA CR-3251, Vol. 1, Ver. 3.0, Revision 1, 1991.

[15] Bonner E, Clever W and Dunn K. Aerodynamic preliminary analysis system 2 part 1 - theory. NASA CR-182076, 1991.

[16] Peterson J. A comparison of experimental and theoretical results for the compressible turbulent-boundary-layer skin friction with zero pressure gradient. NASA TN-D-1795, 1963.

[17] Chen S, Cowan C and Grant P. Orthogonal least squares algorithm for radial basis function networks. *IEEE Transactions on Neural Networks*, Vol. 2, No. 2, pp 302-309, 1991.

[18] Yokoyama N, Suzuki S and Tsuchiya T. Construction and evaluation of RBF network approximation for space plane's aerodynamics. *Proceedings of the 41st Aircraft Symposium*, Paper No. IS17-11, 2003.